IOP Publishing Journal of Physics D: Applied Physics

J. Phys. D: Appl. Phys. **52** (2019) 015303 (7pp) https://doi.org/10.1088/1361-6463/aae67b

Spin current generation by thermal gradient in graphene/*h*-BN/graphene lateral heterojunctions

Peng Jiang[1,2], Xixi Tao[1,2], Lili Kang[1,2], Hua Hao[1], Lingling Song[3], Jie Lan[4], Xiaohong Zheng[1,2,5], Lei Zhang[5,6] and Zhi Zeng[1,2]

[1] Key Laboratory of Materials Physics, Institute of Solid State Physics, Chinese Academy of Sciences, Hefei 230031, People's Republic of China
[2] University of Science and Technology of China, Hefei 230026, People's Republic of China
[3] School of Electronic Science and Applied Physics, Hefei University of Technology, Hefei 230009, People's Republic of China
[4] School of Physics and Electronic Engineering, Jiangsu Normal University, Xuzhou 221116, People's Republic of China
[5] State Key Laboratory of Quantum Optics and Quantum Optics Devices, Institute of Laser Spectroscopy, Shanxi University, Taiyuan 030006, People's Republic of China
[6] Collaborative Innovation Center of Extreme Optics, Shanxi University, Taiyuan 030006, People's Republic of China

E-mail: xhzheng@theory.issp.ac.cn and zhanglei@sxu.edu.cn

Received 23 July 2018, revised 1 October 2018
Accepted for publication 5 October 2018
Published 25 October 2018

Abstract

Electron transport driven by a temperature gradient in a transport junction constructed by connecting a zigzag hexagonal boron nitride (*h*-BN) nanoribbon between two graphene nanoribbons (Gr/BN/Gr) is studied by density functional calculations and non-equilibrium Green's function method. When the zigzag-edged graphene nanoribbons are in the ferromagnetic configuration, the BN barrier introduces a spin-dependent scattering and causes an 'X'-type spin-dependent transmission functions around the Fermi level at equilibrium. In a linear response approximation, this gives rise to a Seebeck thermopower with opposite signs for different spins. It drives electrons with different spins to flow in opposite directions under a finite temperature gradient. Calculations show that the charge current is zero while spin current is not, thus pure spin current is generated. These findings suggests the great importance of BN barrier in the generation of thermal spin current using graphene and the idea should be taken into consideration in the design of spintronic devices using two dimensional materials.

Keywords: spin current, graphene/ h-BN/graphene lateral heterojunction, temperature gradient, first principles

(Some figures may appear in colour only in the online journal)

1. Introduction

Spintronics, which works on the electron spin instead of charge to build new electronic devices, has attracted intensive interests since the discovery of giant magnetoresistance effect due to the great advantages of spin manipulation, such as fast speed, low energy consumption and high integration densities [1, 2]. Thus far, many effects related with spin transport, such as spin filtering [3, 4], spin switching [5–8], and spin current [9–17], have initiated great interests. Especially, spin current, a very important physical quantity in spintronics, and characterized by the opposite flow direction for different spins, has been intensively studied. Importantly, how to generate spin current has been the focus of numerous studies for many

years. Up to now, there are several schemes or mechanisms for producing spin current, such as spin Hall effect induced by spin–orbit coupling [10, 11, 18], optical injection [19], current injection from a ferromagnet to a normal metal [20], adiabatic quantum pumping [12, 13], voltage control in three-terminal devices [14], macroscopic phase difference control in intrinsically spin–orbit coupled superconductor/ferromagnet/superconductor (S/F/S) Josephson junctions [15, 16], Strain-controlled spin pumping [17], and the superconducting proximity effect due to Andreev reflection in hybrid F/S system [7]. Recently, there emerges a new field, namely, spin caloritronics [21, 22], which combines both thermoelectrics and spintronics and mainly studies the interaction between spin, charge and heat in materials. An important effect in a spin caloritronic device is the spin-dependent Seebeck effect (SDSE), which features different Seebeck thermopower for different spins in spin polarized systems [23, 24]. It has been shown that the thermoelectric field induced by a temperature gradient may drive the electrons to flow either from the hot lead to the cold lead or from the cold lead to the hot lead, depending on the sign of the thermopower S [25]. Interestingly, in certain spin polarized systems, the sign of thermopower can be positive for one spin and negative for the other simultaneously [26–28]. With this feature, SDSE was suggested as an alternative way for spin current generation [29].

It is well known that low dimensionality leads to fascinating properties due to quantum confinement effect. In particular, two dimensional (2D) materials have initiated extensive investigation since graphene was successfully fabricated in 2004 [30], followed by the discovery of many other 2D materials, such as, hexagonal boron nitride sheet (*h*-BN) [31], transition-metal dichalcogenides (TMDs) [32], monolayer black phosphorus (MBP) [33], silicene [34, 35], and others [36–41]. One dimensional(1D) form of them, namely, cutting them into nanoribbons, often results in different properties from their bulk. As the first member of 2D material family fabricated experimentally, graphene is considered as a potential candidate for spintronic devices due to its excellent properties, such as long spin diffusion paths, high carrier mobility and extreme flexibility [42–44]. Especially, graphene nanoribbons with zigzag edges (ZGNRs) have two magnetic states, namely, ferromagnetic (FM) and antiferromagnetic (AFM) states, which originate from different magnetic couplings between the edges. Although AFM state is the ground state of ZGNRs, it can transform into FM state under the condition of magnetic filed, thus the properties for the FM state of ZGNRs have been extensively studied [45–47]. In addition, *h*-BN is also a one-atom-thick material structurally quite similar to graphene with one sublattice occupied by B atoms and the other by N atoms [48, 49]. Distinct from graphene, monolayer *h*-BN is an insulator with a wide band gap about 5.9 eV. Similarly to graphene, *h*-BN sheet can also be cut into nanoribbons with zigzag or armchair edges. Previous studies have shown that *h*-BN nanoribbons (BNNRs) are stable under high temperature and more resistant to oxidation than graphene. Moreover, due to the very small lattice mismatch and the marked difference of electronic properties between graphene and *h*-BN sheet, hybrid heterostructures composed of graphene and *h*-BN nanoribbons (Gr-BN) have attracted great attention both theoretically and experimentally [50–53]. On one hand, monolayer in-plane heterostructures consisting of graphene and *h*-BN have been synthesized [51, 54]. On the other hand, theoretical studies demonstrate that monolayer GNR-BNNR heterostructures exhibit new electronic and magnetic properties different from both the pristine graphene and *h*-BN sheet. This provides the possibility of tuning the spin transport of GNRs by constructing Gr-BN heterstructures [52, 55].

To date, many studies of thermally inducing spin transport and MR effect in graphene and graphene nanoribbons (GNRs) have been reported [29, 55–59]. However, there are still no investigations about thermal spin current in GNRs, since perfect GNRs are generally not suitable for thermally inducing spin current due to the spin degeneracy of electron transmission around the Fermi level. To break the spin degeneracy, it is desirable to introduce spin-dependent scattering that leads to opposite slopes in the transmission functions of different spin channels [27]. Motivated by the successful synthesis and the interesting spin properties of monolayer hybrid Gr-BN structures, in this work, we propose a lateral heterostructure constructed by connecting a zigzag hexagonal BNNR segment between two semi-infinite ferromagnetic ZGNRs (abbreviated as Gr/$(BN)_n$/Gr,with n denoting the number of primitive cells of the BNNR). One possible way to fabricate this lateral structure is to mechanically cut the graphene/ *h*-BN hybrid monolayer with the tip of a scanning tunneling microscope, which has been demonstrated for the fabrication of GNRs out of graphene [60]. We treat this heterostructure as a two-probe device, with the BNNR segment acting as the scattering region and the GNRs as the leads. The BNNR works as a potential barrier, thus the electrons incoming from one lead will be scattered before entering the other lead. Although the BNNR is non-magnetic, it will provide spin-dependent scattering potentials when it lies in a spin polarized environment. By carrying out density functional theory (DFT) calculations combined with a non-equilibrium Green's function (NEGF) technique, the thermal spin transport of Gr/$(BN)_n$/Gr heterostructures under temperature gradient is studied and a spin-dependent Seebeck effect is obtained. Interestingly, the Seebeck thermopowers for the two spins have opposite signs and nearly equal magnitudes, which is promising for generating pure spin current thermally.

The rest of this paper is organized as follows: in section 2, we present our proposed system, computational details and the theoretical formalism. The numerical results of spin-polarized transport are discussed in section 3. Finally, the paper is summarized in section 4.

2. Theory and method

The heterostructure is constructed by connecting a 8-BNNR between two 8-ZGNRs, where '8' denotes the number of zigzag carbon or BN chains along the transport direction. For BNNRs and GNRs with dangling bonds, the edges are generally not stable and tend to be reconstructed, thus the dangling bonds of *h*-BN and graphene nanoribbon edge atoms

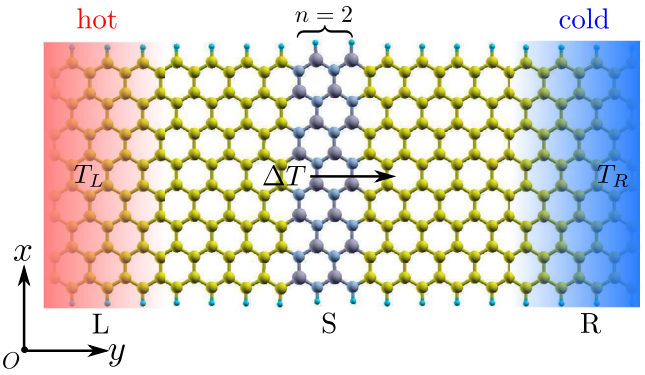

Figure 1. The structure Gr/$(BN)_n$/Gr transport junction with $n = 2$. It is divided into three parts: left lead (L), right lead (R) and scattering region (S). T_L and T_R are the temperature of the left and right lead, and temperature gradient $\Delta T = T_L - T_R$. The arrow indicates the transport direction. Here, $n = 2$ denotes that the h-BN part contains 2 unit cells, with length of $2.46 \times 2 = 4.92$ Å.

are usually terminated by H atoms [61, 62]. The model is divided into three parts: left lead(L), right lead(R) and scattering region(S), which is shown in figure 1. Due to the very small lattice mismatch and the similar lattice structure of graphene (bond length: 1.42 Å) and h-BN (bond length: 1.46 Å), the lattice constant of h-BN ribbons is taken to be the same as the ZBNNRs (2.46 Å). Thus, for the case shown in figure 1 with $n = 2$, the actual size of the BN is 4.92 Å in length and 15.6 Å in width. All calculations for electronic structure and quantum transport are performed by the first-principles software package NanoDcal which is based on density functional theory (DFT) combined with nonequilibrium Green's function (NEGF) method [63]. The generalized gradient approximation (GGA) with Perdew–Burke–Ernzerhof (PBE) [64] is used for the exchange-correlation potential and a double zeta polarization basis set (DZP) is adopted for expanding the electron wave functions. The cutoff energy is set to 200 Ry and the mesh grid of the k-space of the leads is $1 \times 1 \times 100$. The vacuum layer is set to 16 Å to eliminate interaction from the neighbors. The structure is fully relaxed by a conjugate gradient method until the absolute value of force on each atom is less than 0.01 eV $Å^{-1}$.

In the framework of Landauer-B *ü*ttiker formalism [65], the spin-dependent electric current is given by

$$I_\sigma = \frac{e}{h}\int [f_L(\varepsilon, T_L) - f_R(\varepsilon, T_R)]\tau_\sigma(\varepsilon)d\varepsilon \qquad (1)$$

where e is the electron charge and h is the Planck constant; f_α is the Fermi distribution function of the α lead, and T_α is the temperature of the α lead; $\tau_\sigma(\varepsilon)$ is the spin-dependent transmission coefficient, calculated by [66, 67]

$$\tau_\sigma(\varepsilon) = Tr[\Gamma_L(\varepsilon)G^r(\varepsilon)\Gamma_R(\varepsilon)G^a(\varepsilon)]_\sigma. \qquad (2)$$

Here, σ is spin index ($\sigma = \uparrow, \downarrow$) and by default, in the study of systems with collinear spins, the direction of quantization axis is generally chosen as the z axis of the coordinate system used, which is perpendicular to the ribbon atomic plane in this work. $G^r(G^a)$ is retarded (advanced) Green's function, and are calculated by

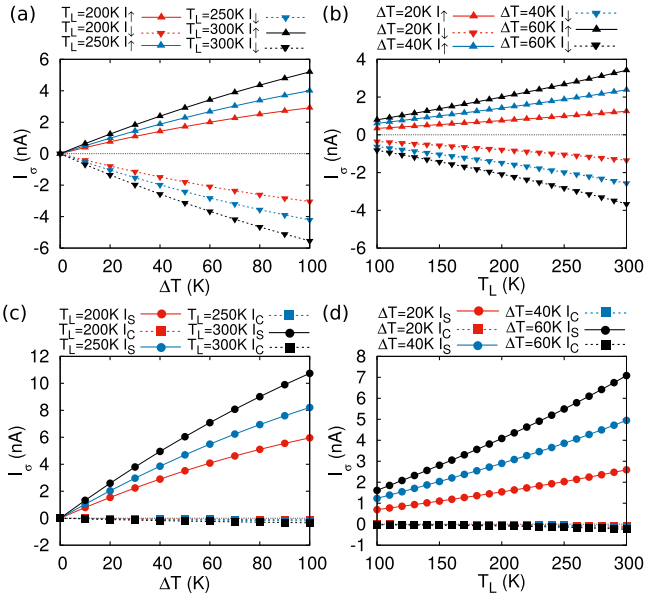

Figure 2. Spin-dependent currents $I_\sigma(\sigma = \uparrow, \downarrow)$ for channel length $n = 2$ as a function of: (a) ΔT for $T_L = 200$, 250 and 300 K; (b) T_L for $\Delta T = 20$, 40 and 60 K. (c) and (d): total charge currents I_c and spin currents I_s obtained from (a) and (b), respectively.

$$G^{r,a}(\varepsilon) = [\varepsilon S - H - (\Sigma_L^{r,a} - \Sigma_R^{r,a})]^{-1} \qquad (3)$$

where S and H are the overlap matrix of the localized basis sets and the Hamiltonian matrix of the central region, $\Sigma_\sigma^{r,a}$ describes the retarded and advanced self-energy of lead σ. $\Gamma_{L/R} = i(\Sigma_{L/R}^r - \Sigma_{L/R}^a)$ are the linewidth functions of the leads, describing the coupling between the leads and the central region. The imbalance on the left and right lead due to a temperature difference $\Delta T = T_L - T_R$ may lead to spin-dependent currents, even with opposite flow directions for different spins, which depends on the feature of spin polarized transmission spectrum.

3. Results and discussion

In this work, we only consider the FM state of ZGNRs parallel configuration (PC), which is achievable by applying a uniform magnetic field to the whole system. The temperature in the left lead and right lead are set as T_L and T_R, respectively, where $T_L > T_R$ is supposed and the temperature difference between two leads is $\Delta T = T_L - T_R$. In all numerical transport calculations, the direction of the spin carriers transport is along y axis and the positive direction is defined as $+y$ direction (that is, the direction from hot side to cold side).

Firstly we study the thermal spin-dependent currents I_σ as a function of ΔT for various T_L and as a function of T_L for different ΔT at $n = 2$, as shown in figures 2(a) and (b). We find that the thermally induced current of both the spin-up $I_\uparrow$ and spin-down $I_\downarrow$ increases almost linearly with the temperature. Meanwhile, $I_\uparrow$ and $I_\downarrow$ always flow in opposite direction under a temperature gradient, indicating there is spin-dependent Seebeck effect in the Gr/$(BN)_2$/Gr junction.

More interestingly, as shown in figures 2(c) and (d), the magnitude of total charge current I_c (defined as $I_c = I_\uparrow + I_\downarrow$) always nearly equals to zero while spin current (defined as $I_c = I_\uparrow - I_\downarrow$) increases linearly with increasing T_L or ΔT. It demonstrates that pure spin current is generated at various T_L and ΔT. Thus, Gr/$(BN)_2$/Gr heterostructure is a good and stable pure spin current generator.

To make clear the physical mechanism of the thermal spin current effect, we analyze the transmission spectra $\tau_\sigma(\varepsilon)$ of the Gr/$(BN)_2$/Gr heterostructure (see figure 3(b)) and the difference in the Fermi distribution functions $D(\varepsilon) = f_L(T_L) - f_R(T_R)$ of the two leads(see figures 3(c) and (d)) since these are the two factors determining the magnitude of current according to equation (2). The transport properties of the device are dominated by the electrons around E_F, which can be seen from the $D(\varepsilon)$ distribution so we mainly focus on transmission $\tau(\varepsilon)$ in the small energy region about 0.3 eV around the Fermi level. When $\Delta T = T_L - T_R$ is not zero, the factor $D(\varepsilon)$ is also not zero and is an odd function of electron energy. It is seen that the magnitude of $D(\varepsilon)$ increases versus ΔT for a given T_L from figure 3(c). In contrast, for a given ΔT, the magnitude of $D(\varepsilon)$ decreases and its width increases versus T_L. The net current of each spin component can be divided into two contributions, one from the electrons with energy lower than the Fermi level ($I_\sigma(\varepsilon \leqslant E_F)$) and the other from electrons with energy higher than the Fermi level ($I_\sigma(\varepsilon \geqslant E_F)$). From figures 3(c) and (d), $I_\sigma(\varepsilon \geqslant E_F)$ goes to right while $I_\sigma(\varepsilon \leqslant E_F)$ goes to left. Since $D(\varepsilon)$ is an odd function of ε, the sign (direction) of the net spin-dependent current I_σ depends on the difference of the spin-dependent transmission spectra below and above the Fermi level. Figure 3(b) shows that spin-up transmission coefficient $\tau_\uparrow$ decreases and the spin-down transmission coefficient $\tau_\downarrow$ increases versus ε, thus $I_\uparrow$ is negative while $I_\downarrow$ is positive. Because of the transmission spectra shows symmetric behaviors for two spins around Fermi level, the magnitude of $I_\uparrow$ and $I_\downarrow$ is nearly identical, and pure spin current is produced by a temperature gradient in the device.

As a matter of fact, thermoelectric effect can be described by the Seebeck thermopower, which is defined by the voltage difference needed to neutralize the temperature induced current divided by the temperature difference [68, 69], namely, $S_\sigma = \frac{U_\sigma}{\Delta T}$. The sign of S_σ determines the flow direction of electron under a temperature gradient, which is not necessarily from the hot side to the cold side, as expected from intuition. With some derivation, it is related to the transmission function τ_σ by the following relation at low temperature [25, 27, 68]:

$$S_\sigma(\mu) = -\frac{k_B \pi^2 T}{3e} \frac{\frac{\partial \tau_\sigma(\varepsilon)}{\partial \varepsilon}|_{\varepsilon=\mu}}{\tau_\sigma(\mu)}. \quad (4)$$

It clearly shows that it is linearly proportional to the slope of τ_σ, namely, $\frac{\partial \tau_\sigma(\varepsilon)}{\partial \varepsilon}$. Thus, in order to get spin current in a system, we need to achieve transmission functions for the two spins with opposite slopes, namely, an 'X' shape around the Fermi level, which is exactly the case in our study.

In order to understand the decrease/increase of spin up/down channel around the Fermi level in the transmission function, the local density of states (LDOS) in the energy range $[-2.0, +2.0]$ eV are studied and its average over the transverse directions is shown in figures 4(a) and (b). It indicates that, different from the pristine *h*-BN nanoribbon with a large band gap (∼5.9 eV), in the junction, the *h*-BN nanoribbon contributes finite density of states around the Fermi level, due to the strong hybridization with the graphene nanoribbons. The LDOS around the *h*-BN units is shown more clearly in figures 4(c) and (d). We see that at each *y* position, the LDOS of spin up channel decreases and that of spin down channel increases. The total density of states of the *h*-BN units is shown in figure 4(e), from which we see clearly a 'X' shape, which fully explains the 'X' shape in the transmission shown in figure 3(b).

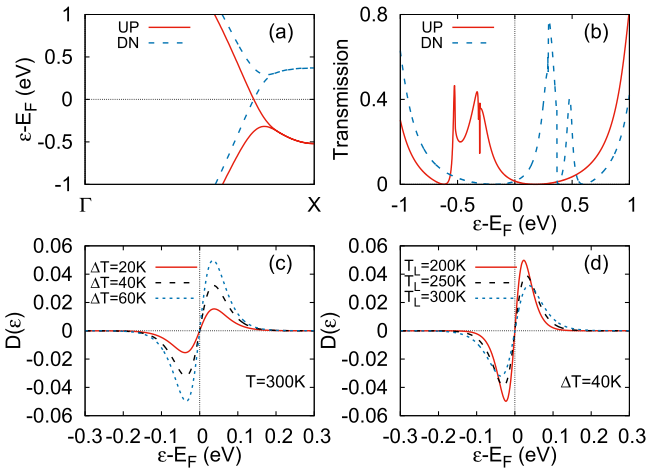

Figure 3. (a) The band structure of FM graphene. (b) The spin polarized transmission function for Gr/$(BN)_2$/Gr at $n = 2$. (c) $D(\varepsilon) = f_L(T_L) - f_R(T_R)$ as a function of energy E and finite $T = 300$ K for various ΔT. (d) $D(\varepsilon)$ as a function of energy ε and with finite temperature gradient $\Delta T = 40$ K for various T.

In the following, the effect of *h*-BN nanoribbon length is studied. Figures 5(a) and (b) show the spin-dependent transmission function with $n = 3$ and $n = 1$, respectively. We find that both spin-up and spin-down channels in the transmission spectra have opposite slope around the Fermi level for different lengths of BN nanoribbon. It implies that spin current can be obtained, which is confirmed by the nearly zero charge current and finite spin current shown in figures 5(c) and (d). Compared with $n = 2$ case (figure 2(a)), the spin current in the $n = 3$ case (figure 5(c)) is much smaller due to the increase in the BN length. It is natural to see the directions of spin current in these two cases are the same due to the similar feature of spin-dependent transmission function around the Fermi level. We can expect that the same conclusion will be obtained with the increase of BN length, except that the magnitude of the spin current will become smaller. In the $n = 1$ case, we also observe spin current and the magnitude of the spin current is much larger. However, it is different from the $n \geqslant 2$ cases since the direction of the spin current is opposite, which arises from the feature of the transmission function around the Fermi level where the spin up channel increases while the the spin down channel decreases. The minimum appears at −0.2 eV and 0.2 eV for spin up and spin down channels, respectively, different from the $n \geqslant 2$ cases.

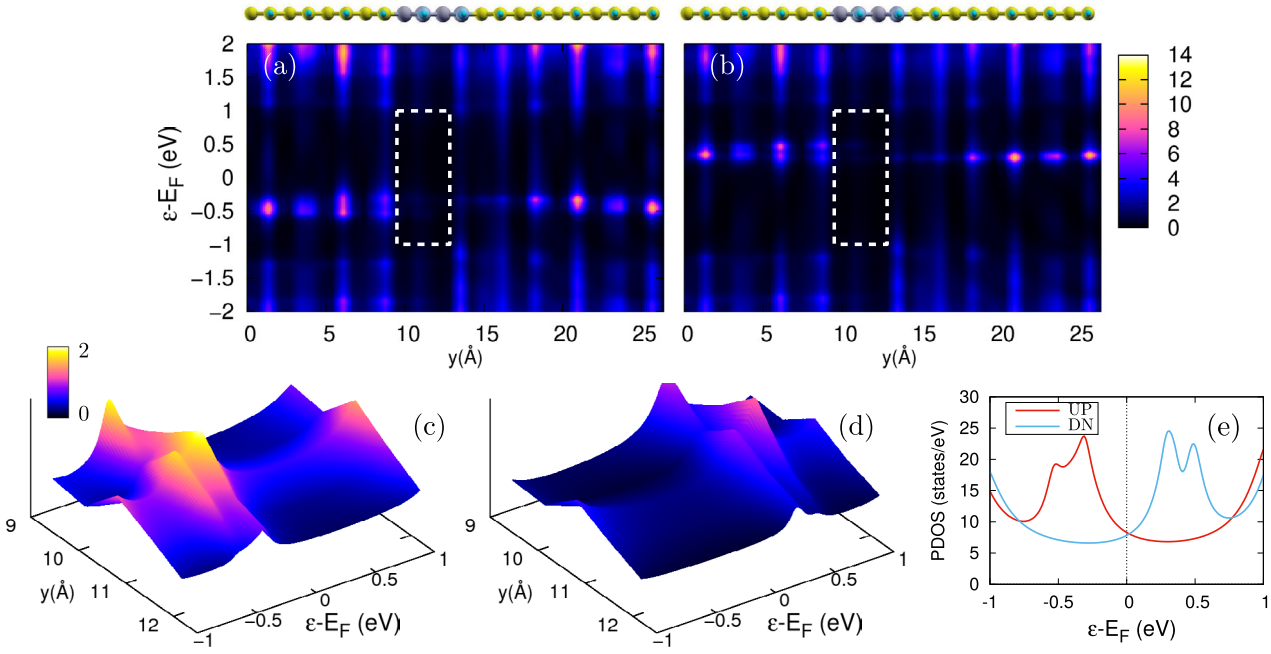

Figure 4. The LDOS averaged over the transverse directions of the whole device in energy range $[-2.0, +2.0]$ eV with channel length $n = 2$ for: (a) spin up and (b) spin down. (c), (d) The local distribution of LDOS around the *h*-BN units indicated by white dashed line box in (a) and (b), respectively. (e) The spin resolved total density of states of the *h*-BN units.

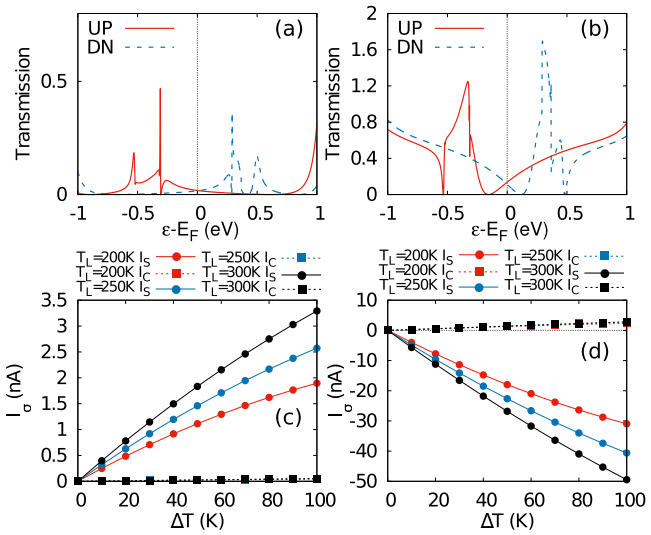

Figure 5. The spin-dependent transmission function for Gr/$(BN)_n$/Gr at $n = 3$ (a) and $n = 1$ (b), respectively; and the spin currents and charge currents as a function of ΔT for various T_L at $n = 3$ (c) and $n = 1$ (d).

Now we briefly discuss the detection of spin current. Currently, the detection of a pure spin current is mostly indirect, such as being achieved through the measurement of effects induced by the spin current such as inverse spin Hall effect [20, 70, 71], spin-current induced second-harmonic optical effects [72] and spin-torque driven magnetization precession [73, 74], etc. Recently, Li *et el* made a direct detection of spin current by x-ray magnetic circular dichroism [75]. These methods may give hints on how to experimentally measure and detect the spin-imbalance and spin-current explored in this work.

Finally, another interesting feature in the transport properties is the two Fano-like resonance peaks in the transmission function around the Fermi level E_F in all the studied cases, but more clearly in the $n = 3$ case (figure 5(a)): one peak at -0.31 eV in the spin-up channel and the other one at 0.29 eV in the spin-down channel. It is well known that Fano resonance arises from the interaction of a static state and a propagating state. From the band structure shown in figure 3(a), we see that at these two energy points, there are two states, with a finite group velocity for one and exactly a zero group velocity for the other, namely, the local minimum or maximum point in the corresponding band. Thus the interference between these two states gives rise to the Fano resonance.

4. Summary

In summary, we have studied the thermal spin transport in Gr/$(BN)_n$/Gr heterostructure. It is found that the flow directions of $I_\uparrow$ and $I_\downarrow$ are opposite and the magnitudes of the spin-up and spin-down current are nearly identical for all the $n = 1$, 2 and 3 cases. This indicates that nearly pure spin current can always be generated at different T_L and ΔT. These findings demonstrate that insertion of BN segment is a very efficient way for generating spin current in graphene nanoribbons using a temperature gradient and the Gr/BN/Gr heterostructures have potential application in the future spin caloritronics.

Acknowledgment

We gratefully acknowledge financial support by the National Natural Science Foundation of China under Grant Nos. 11574318 (XZ), 11704232 (LZ), 11374301 (HH), 21503061

(LS) and 11647147 (JL); the Major/Innovative Program of Development Foundation of Hefei Center for Physical Science and Technology (under Grant No. 2016FXCX003) (XZ); Shanxi Science and Technology Department (No. 201701D121003) (LZ) and the Program of State Key Laboratory of Quantum Optics and Quantum Optics Devices (No: KF201810) (XZ and LZ); National Key R&D Program of China under Grants No. 2017YFA0304203 (LZ); Shanxi Province 100-Plan Talent Program (LZ). Calculations were performed in Center for Computational Science of CASHIPS, the ScGrid of Supercomputing Center and Computer Network Information Center of Chinese Academy of Sciences.

ORCID iDs

Peng Jiang https://orcid.org/0000-0002-4291-608X
Xiaohong Zheng https://orcid.org/0000-0002-3027-1042
Lei Zhang https://orcid.org/0000-0002-8634-8037

References

[1] Wolf S, Awschalom D, Buhrman R, Daughton J, Von Molnar S, Roukes M, Chtchelkanova A Y and Treger D 2001 *Science* **294** 1488
[2] Awschalom D D and Flatté M E 2007 *Nat. Phys.* **3** 153
[3] Zheng X, Chen X, Zhang L, Xiao L, Jia S, Zeng Z and Guo H 2017 *2D Mater.* **4** 025013
[4] Tao X, Hao H, Wang X, Zheng X and Zeng Z 2016 *Appl. Phys. Lett.* **108** 233106
[5] Tagirov L R 1999 *Phys. Rev. Lett.* **83** 2058
[6] Halterman K, Valls O T and Alidoust M 2013 *Phys. Rev. Lett.* **111** 046602
[7] Niu Z 2012 *Appl. Phys. Lett.* **101** 062601
[8] Halterman K and Alidoust M 2016 *Supercond. Sci. Technol.* **29** 055007
[9] Sun Q F and Xie X C 2005 *Phys. Rev.* B **72** 245305
[10] Hirsch J E 1999 *Phys. Rev. Lett.* **83** 1834
[11] Mishchenko E G, Shytov A V and Halperin B I 2004 *Phys. Rev. Lett.* **93** 226602
[12] Zhang Q, Chan K S and Lin Z 2011 *Appl. Phys. Lett.* **98** 032106
[13] Souma S and Ogawa M 2014 *Appl. Phys. Lett.* **104** 183103
[14] Ma Z, Wu R L, Yu Y B and Wang M 2014 *J. Appl. Phys.* **116** 043706
[15] Alidoust M and Halterman K 2015 *New J. Phys.* **17** 033001
[16] Alidoust M and Halterman K 2015 *J. Phys.: Condens. Matter* **27** 235301
[17] Mohammadkhani R, Abdollahipour B and Alidoust M 2015 *Eur. Phys. Lett.* **111** 67005
[18] Raimondi R, Gorini C, Dzierzawa M and Schwab P 2007 *Solid State Commun.* **144** 524
[19] Hübner J, Rühle W W, Klude M, Hommel D, Bhat R D R, Sipe J E and van Driel H M 2003 *Phys. Rev. Lett.* **90** 216601
[20] Valenzuela S O and Tinkham M 2006 *Nature* **442** 176
[21] Bauer G E W, Saitoh E and Wees B J V 2010 *Solid State Commun.* **150** 459
[22] Bauer G E, Saitoh E and Van Wees B J 2012 *Nat. Mater.* **11** 391
[23] Slachter A, Bakker F L, Adam J and Wees B J V 2010 *Nat. Phys.* **6** 879
[24] Dejene F K, Flipse J and Wees B J V 2012 *Phys. Rev. B: Condens. Matter* **86** 6335
[25] Zheng X, Zheng W, Wei Y, Zeng Z and Wang J 2004 *J. Chem. Phys.* **121** 8537
[26] Chen X, Liu Y, Gu B L, Duan W and Liu F 2014 *Phys. Rev.* B **90** 121403
[27] Jiang P, Tao X, Hao H, Song L, Zheng X, Zhang L and Zeng Z 2017 *2D Mater.* **4** 035001
[28] Jiang P, Tao X, Hao H, Song L, Zheng X and Zeng Z 2017 *RSC Adv.* **7** 28124
[29] Yu X Q, Zhu Z G, Su G and Jauho A P 2015 *Phys. Rev. Lett.* **115** 246601
[30] Novoselov K S, Geim A K, Morozov S V, Jiang D, Zhang Y, Dubonos S V, Grigorieva I V and Firsov A A 2004 *Science* **306** 666
[31] Zhi C, Bando Y, Tang C, Kuwahara H and Golberg D 2009 *Adv. Mater.* **21** 2889
[32] Novoselov K, Jiang D, Schedin F, Booth T, Khotkevich V, Morozov S and Geim A 2005 *Proc. Natl Acad. Sci. USA* 102 10451
[33] Li L, Yu Y, Ye G J, Ge Q, Ou X, Wu H, Feng D, Chen X H and Zhang Y 2014 *Nat. Nanotechnol.* **9** 372
[34] Cahangirov S, Topsakal M, Aktrk E, Sahin H and Ciraci S 2009 *Phys. Rev. Lett.* **102** 236804
[35] Vogt P, De Padova P, Quaresima C, Avila J, Frantzeskakis E, Asensio M C, Resta A, Ealet B and Le Lay G 2012 *Phys. Rev. Lett.* **108** 155501
[36] Mannix A J *et al* 2015 *Science* **350** 1513
[37] Yang J H, Zhang Y, Yin W J, Gong X, Yakobson B I and Wei S H 2016 *Nano Lett.* **16** 1110
[38] Elias D *et al* 2009 *Science* **323** 610
[39] Malko D, Neiss C, Viñes F and Görling A 2012 *Phys. Rev. Lett.* **108** 086804
[40] Vaughn D D II, Patel R J, Hickner M A and Schaak R E 2010 *J. Am. Chem. Soc.* **132** 15170
[41] Zhao L D, Lo S H, Zhang Y, Sun H, Tan G, Uher C, Wolverton C, Dravid V P and Kanatzidis M G 2014 *Nature* **508** 373
[42] Bolotin K I, Sikes K J, Jiang Z, Klima M, Fudenberg G, Hone J, Kim P and Stormer H L 2008 *Solid State Commun.* **146** 351
[43] Geim A K and Novoselov K S 2007 *Nat. Mater.* **6** 183
[44] Geim A K 2009 *Science* **324** 1530
[45] Zheng X H, Wang X L, Huang L F, Hao H, Lan J and Zeng Z 2012 *Phys. Rev. B: Condens. Matter* **86** 081408(R)
[46] Bai J, Cheng R, Xiu F, Liao L, Wang M, Shailos A, Wang K L, Huang Y and Duan X 2010 *Nat. Nanotechnol.* **5** 655
[47] Liu F, Li Y, Liu X and Kang J 2011 *Appl. Phys. Lett.* **99** 243503
[48] Alem N, Erni R, Kisielowski C, Rossell M D, Gannett W and Zettl A 2009 *Phys. Rev.* B **80** 155425
[49] Dean C R *et al* 2010 *Nat. Nanotechnol.* **5** 722
[50] Ilyasov V V, Meshi B C, Nguyen V C, Ershov I V and Nguyen D C 2014 *J. Chem. Phys.* **141** 014708
[51] Ci L, Song L, Jin C, Jariwala D, Wu D, Li Y, Srivastava A, Wang Z F, Storr K and Balicas L 2010 *Nat. Mater.* **9** 430
[52] Liu Y, Wu X, Zhao Y, Zeng X C and Yang J 2011 *J. Phys. Chem.* C **115** 9442
[53] Tao X, Zhang L, Zheng X, Hao H, Wang X, Song L, Zeng Z and Guo H 2018 *Nanoscale* **10** 174
[54] Liu Z, Ma L, Shi G, Zhou W, Gong Y, Lei S, Yang X, Zhang J, Yu J and Hackenberg K P 2013 *Nat. Nanotechnol.* **8** 119
[55] Zhu L, Li R and Yao K 2017 *Phys. Chem. Chem. Phys.* **19** 4085
[56] Ni Y, Yao K, Fu H, Gao G, Zhu S and Wang S 2013 *Sci. Rep.* **3** 1380
[57] Li J, Wang B, Xu F, Wei Y and Wang J 2016 *Phys. Rev.* B **93** 195426
[58] Zeng M, Huang W and Liang G 2013 *Nanoscale* **5** 200

[59] Zuev Y M, Chang W and Kim P 2009 *Phys. Rev. Lett.* **102** 096807
[60] Tapaszto L, Dobrik G, Lambin P and Bio L P 2008 *Nat. Nanotechnol.* **3** 397
[61] Song L L, Zheng X H, Wang R L and Zeng Z 2010 *J. Phys. Chem.* C **114** 12145
[62] Zhang X, Yazyev O V, Feng J, Xie L, Tao C, Chen Y C, Jiao L, Pedramrazi Z, Zettl A and Louie S G 2013 *ACS Nano* **7** 198
[63] Maassen J, Harb M, Michaud-Rioux V, Zhu Y and Guo H 2013 *Proc. IEEE* **101** 518
[64] Perdew J P, Burke K and Ernzerhof M 1996 *Phys. Rev. Lett.* **77** 3865
[65] Imry Y and Landauer R 1999 *Rev. Mod. Phys.* **71** 1
[66] Datta S 1995 *Electronic Transport in Mesoscopic Systems* (New York: Cambridge University Press)
[67] Haug H and Jauho A P 1996 *Quantum Kinetics in Transport and Optics of Semiconductors* (Berlin: Springer)
[68] Proetto C R 1991 *Phys. Rev.* B **44** 9096
[69] Rejec T, Ramšak A and Jefferson J H 2002 *Phys. Rev.* B **65** 235301
[70] Saitoh E, Ueda M, Miyajima H and Tatara G 2006 *Appl. Phys. Lett.* **88** 182509
[71] Kimura T, Otani Y, Sato T, Takahashi S and Maekawa S 2007 *Phys. Rev. Lett.* **98** 249901
[72] Werake L K and Zhao H 2010 *Nat. Phys.* **6** 875
[73] Kiselev S I, Sankey J C, Krivorotov I N, Emley N C, Schoelkopf R J, Buhrman R A and Ralph D C 2003 *Nature* **425** 380
[74] Heinrich B, Tserkovnyak Y, Woltersdorf G, Brataas A, Urban R and Bauer G E 2003 *Phys. Rev. Lett.* **90** 187601
[75] Li J *et al* 2016 *Phys. Rev. Lett.* **117** 076602